Pharmaceutical Sciences, 2025, 31(1), 74-88
doi:10.34172/PS.024.40626
https://ps.tbzmed.ac.ir/

Research Article

Optimization and Enhancement of Oral Bioavailability of Dabrafenib as Nanobubbles Using Quality by Design Approach

Bijili Vijaya Laxmi[1], Darna Bhikshapathi[2,3*], Penakalapati Sailaja Rao[3]

[1]*Research Scholar, Bir Tikendrajit University, Canchipur, Imphal West-795003, Manipur, India.*
[2]*Research Supervisor, Bir Tikendrajit University, Canchipur, Imphal West-795003, Manipur, India.*
[3]*Teegala Ram Reddy College of Pharmacy, Meerpet-500097, Hyderabad, India.*

Article Info

Article History:
Received: 24 Jun 2024
Accepted: 9 Oct 2024
ePublished: 31 Oct 2024

Keywords:
-Box-Behnken design
-Chronic myeloid leukaemia
-Dabrafenib
-Nanobubbles

Abstract

Background: The use of Poly (lactic-co-glycolic acid) (PLGA) nanobubbles (NBs) aimed at functioning as a delivery system that encounter solubility issues for drugs like dabrafenib (DBF), which belonged to the Biopharmaceutical Classification System (BCS) class II category. These specially designed nanobubbles enhanced the drug's solubility, stability, and bioavailability, thus improving the therapeutic effectiveness. Moreover, they offered controlled release characteristics and can potentially enhance drug delivery to tissues or cells, maximizing pharmacological results while reducing adverse effects.

Methods: PLGA NBs were formulated using solvent evaporation and optimized using a Box Behnken design considering process and formulation parameters. The NBs characterization includes particle size, drug loading, entrapment efficiency, in-vitro studies, haemolytic studies, Fourier transform infrared (FTIR) spectroscopy, differential scanning calorimeter (DSC), stability studies, and as well as in-vivo studies in rats.

Results: The optimized nanobubbles (NBs) displayed a particle size (PS) of 190.6 ± 18.4 nm, zeta potential of -21 ± 4.2 mV, and polydispersity index (PDI) of 0.397 ± 0.096. With 87.21 ± 3.8% of entrapment efficiency (EE) and 26.29 ± 4.01% drug loading, in-vitro studies revealed a superior drug release (99%) with ultrasound versus plain drugs (20%). FTIR and DSC studies confirmed no drug-polymer interaction. Scanning Electron Microscopy (SEM) images displayed uniform spherical nanosized particles. Haemolytic activity demonstrated safety, and stability studies indicated no significant changes after 30 days. The nanobubbles exhibited increased C_{max} (4.74) and AUC_{0-t} (6.82), there by promising an enhanced solubility, absorption, and extended half-life.

Conclusion: The current investigation showed that PLGA nanobubbles loaded with dabrafenib have a promising delayed release potential, which might make them a possible treatment alternative for breast cancer.

Introduction

Targeted cancer therapies aim to minimize damage to healthy cells, offering a more precise and effective approach compared to conventional treatments like chemotherapy and radiotherapy.[1] Advancements in cancer-targeted nanotechnologies benefit clinical diagnosis and treatment.[2,3] Multidrug resistance and drug-related complications significantly affect the therapeutic efficacy of cancer drugs.[4] Physically targeted therapies, including High-intensity–focused ultrasound ablation (HIFU),[5] offer alternatives to drug-based cancer treatments,[6] including microwave, photothermal therapy (PTT),[7] radiofrequency,[8] and interstitial laser treatment, which are currently applied in health care scenarios. Exploring novel and cost-effective strategies is essential to address challenges in inducing apoptosis selectively in cancer cells.

Nanoscale drug delivery systems such as light-triggered nanotheranostics (LTN) and laser-tunable plasmonic nanobubbles (PNBs) are promising options.[9] They offer a light-controlled approach for mechanical and optical targeting of tumours, addressing issues related to poor selectivity in traditional methods involving harsh temperature changes.[10]

Novel targeted therapies are needed to overcome challenges in current techniques. Ultrasound (US) is a cost-effective, non-invasive, and precise clinical visual aid that can access distant anatomical targets.[11] Before nanobubble development, overcoming barriers to targeted drug delivery to the central nervous system (CNS) required combining microbubbles (MBs) with transcranial low-intensity focused ultrasound (LIFU).[12]

Nanobubbles (NBs) are minuscule gas-filled spheres that

*Corresponding Author: Darna Bhikshapathi, Email: dbpathi71@gmail.com

measure in the nanometre scale, generally under 1 micron in diameter. Their diminutive size and large surface area render them highly effective for targeted drug delivery applications. By either encapsulating a pharmaceutical within these nanobubbles or binding them to their surfaces, scientists can improve the stability of the drugs and regulate their release. Furthermore, nanobubbles can be directed to particular tissues through external stimuli, thereby enhancing the accuracy and effectiveness of therapeutic interventions. NBs, with a diameter below 1000 nm, are preferred for their enhanced stability and increased drug encapsulation efficiency, resulting in extended bloodstream circulation.[13]

NBs are advanced drug carriers with a gas-filled core and a protein, polymeric, or phospholipid coating. When exposed to high-pressure ultrasound, NBs undergo inertia cavitation, causing shock waves and microjets. This process has significant bioeffects, exerting mechanical impacts on nearby tissues or cells.[14-16] NBs are characterized by their gaseous core, in contrast to nanodroplets, which have a liquid core, and nanoparticles, that are composed of solid material. The presence of gas within NBs imparts a distinctive acoustic property, aids in identification of specialized imaging and characterization methods. Acoustic microscopy and specialized imaging techniques are employed to verify the gas-filled characteristics of nanobubbles, allowing for their differentiation from liquid droplets and solid nanoparticles.[17]

Polymeric NBs, specifically those made from PLGA, offer advantages such as high stability, biodegradability, and ease of chemical modification. These qualities make PLGA a preferred material for various applications, including targeted drug delivery, molecular diagnostics, tissue manipulation, and gene transportation.[18,19]

Superparamagnetic iron oxide (SPIO) nanoparticle-containing PLGA microbubbles reported by Yang *et al.*[18] Micron-sized PLGA carriers, often used in past research, need more targeting capabilities and face challenges in reaching tumour cells through endothelial gaps. Additionally, achieving rapid drug release with standard diagnostic ultrasound is difficult due to the high stability of PLGA.[20,21]

Dabrafenib (DBF) known as Tafinlar, is a Federal Drug Administration (FDA) approved anticancer drug that inhibits B-Raf (BRAF) selectively. It is employed for treating metastatic or unresectable melanoma with the BRAF-V600E mutation.[22] Dabrafenib mesylate salt (DBF. MS) is a BCS Class II drug, demonstrating low solubility and high permeability, and is nearly insoluble in aqueous media within the pH range of 4–8.[23,24] DBF exhibits significant lipophilicity with a log P value of 2.9 and three pK_a values (6.6, 2.2, -1.5). To enhance solubility, new solid forms of DBF are essential.[25]

The aim of this study was to formulate PLGA nanobubbles encapsulating the model drug DBF to enhance the drug delivery in cancer therapy. DBF-loaded NBs were optimized using a double emulsion technique and a Box-Behnken design (BBD). The resulting NBs were characterized for particle size, morphology, and thermal properties. Dissolution and pharmacokinetic studies assessed their kinetics compared to the plain drug.

Methods

Reagents and chemicals

DBF pure drug was acquired from Hetero Drugs Ltd., Hyderabad, India. Sigma Aldrich, US, supplied PLGA 50:50 with an intrinsic viscosity of 0.22 dl/g and mw 25,000. Polyvinyl alcohol (PVA; MW 30,000-70,000) was bought from Sigma Aldrich (St. Louis, MO, USA). Isopropanol and dichloromethane were acquired from S.D. Fine Chemicals, Hyderabad, and Acetonitrile from Qualigens, India. The cells were purchased from NCS Pune, Maharashtra, India. All the media components were purchased from Gibco, USA, and Invitrogen, USA.

Dabrafenib nanobubbles (DBF NBs) formulation development and optimization

PLGA-loaded DBF NBs were formulated using solvent evaporation, following a reported procedure with minor modifications.[26] PLGA was dissolved in dichloromethane (DCM), forming a single-phase solution. After adding DBF to create a dispersion, the mixture underwent two minutes of sonication. The above dispersion was then added to a 2.5% PVA (polyvinyl alcohol) solution, subjected to high-speed homogenizer (IKA T 25) for 10 minutes, at an rpm of 12,000 followed by probe sonication for 1 minute. Later the solvent extraction (DCM) involved by adding a 2.5% v/v isopropanol solution and stirring for 5 h. The resulting formulation was centrifuged, and the precipitate was rinsed three times with deionized water. The nanobubbles were freeze-dried for 36 h, and C_3F_8 (Octafluoropropane) gas was introduced for 1 minute before sealing the vials with caps.[27]

PLGA-DBF NBs optimization employed a three-factor, three-level BBD with 15 experimental runs, including three replicated centre points. Independent variables (homogenization duration, homogenization speed, stabilizer concentration) varied at low (-1), middle (0), and high (1) levels. The drug-to-PLGA ratio remained constant at 0.1:1 (w/w). Dependent variables included PS, PDI, and EE. Ranges for these variables were detailed in Table 1. Response surface analysis, using Design Expert® tools (Version 12, Stat-Ease Inc., Minneapolis, MN), was conducted with Response Surface Charts and contour (2D) plots.).[28,29] The QTPP and CQAs were mentioned in Table S1 (Supplementary Data).

HPLC (high-performance liquid chromatography) analysis

A Shimadzu HPLC system with a Symmetry ODS C18 column (250 x 4.6 mm, 5-micron particle size) and Diode Array APG-M20 detector was used for chromatographic separation. UV absorbance of DBF was measured at 224 nm, and a highly linear calibration curve ($R^2 > 0.999$) was

Table 1. Factors influencing the experiment's design (drug amount is 30 mg).

	Variables	Levels		
		Low (-1)	Medium (0)	High (+1)
A	Stabilizer Concentration (SC)	0. 5	1.50	2.50
B	Homogenization Speed (HS, RPM)	10000	15000	20000
C	Homogenization Duration (HD, min)	5	7.50	10
	Replies		**Restrictions**	
X	Particle size (PS)		Minimize	
Y	Polydispersity index (PDI)		Minimize	
Z	Entrapment efficiency (EE)		Maximum	

achieved by spiking DBF. The mobile phase (methanol and 0.01 M disodium hydrogen phosphate buffer, 80:20, v/v, pH :7.4) was degassed using ultrasonication after filtering through a 0.45 µm membrane. Operating in an isocratic mode at 0.8 mL/min, 20 µL samples were introduced and examined at a wavelength of 224 nm.[30]

DBF for the primary stock (1 mg/mL) was weighed, and a calibration curve (0.250 to 200 ng/mL) was created using a 100 µg/mL secondary stock. Sorafenib (internal standard) was also weighed for this process. A calibration curve (0.250 to 400 ng/mL) was also generated using a secondary stock of 100 µg/mL.

The extraction of a sample for bioanalysis

DBF was separated from plasma samples using the protein precipitation procedure. Plasma (50 µL) was mixed with acetonitrile (250 µL), vortexed, and then centrifuged at 8500 rpm for 10 minutes. The supernatant was analysed using chromatography at a λ_{max} of 224 nm.[30]

Characterization and evaluation

Measurements of particle size (PS), PDI, and zeta potential (ZP)

Using a Malvern zeta sizer (Malvern Instrument, UK), dynamic light scattering (DLS) theory was used to calculate the PS, PDI, and ZP of DBF NBs after ten-fold dilution of the sample with double-distilled water.[31]

Entrapment efficiency (EE) and load capacity (LC))

EE and LC were evaluated by dissolving DBF-loaded nanobubbles (NBs) in dichloromethane. The solution was sonicated for 12 minutes to dissolve the complex. After dilution, HPLC analysis was performed, detecting the DBF at 224 nm. This analytical method aimed to determine the presence and concentration of DBF in the nanobubble formulation, calculated using specific formulae.[32]

$$\%Drug\ Entrapment\ efficiency = \frac{Total\ amount\ of\ the\ drug - free\ drug}{Total\ amount\ of\ drug} \times 100$$

$$\%Loading\ capacity = \frac{Total\ amount\ of\ the\ drug - free\ drug}{Weight\ of\ the\ nanobubble\ formulation\ taken} \times 100$$

Fourier Transform Infrared Spectroscopy (FTIR)

The spectrum of FTIR was obtained using spectroscopy (Bruker Optics, model: Tensor 27), Germany.[33] The drug in its pure form, the drug in its physical mixture (PM), and the optimized NBs were all analysed at wave numbers 4000-450 cm^{-1} with a resolution of 1 cm^{-1}.

Differential Scanning Calorimetry (DSC)

DSC was employed to ascertain the drug's physical structure and the potential for chemical interactions with the excipients. Thermograms of the drug, PM, and NBs formulations were acquired in an environment of nitrogen utilizing a DSC calorimeter (DSC-60, Kyoto, Japan) heated at a rate of 5°C/min over a 200 °C temperature range.

Morphology of the NBs

Using a Quanta FESEM (Field emission scanning electron microscopy-250), the structure of the nanobubbles was photographed. Before the examination, the sample was sputter coated with Au using an ion sputter and placed over double-sided adhesive carbon tape, then mounted over aluminium pin stubs. Analysis of the samples was done at a working distance of 10 mm, 500–10,000 times magnification, and 30 kV accelerating voltage.

Drug release

The DBF drug release values from the NBs with and without ultrasonography at 37 °C were performed using the dialysis bag method. A precise amount of 4 mg of drug-loaded NBs were added to 4 mL of phosphate buffer solution at a pH of 7.4. This combination was then placed inside a dialysis bag, that was tightly sealed at both ends. Following this, the dialysis bag was positioned within a sealed container that contained 25 mL of the identical buffer solution. The container was placed in a shaker maintained at a constant temperature at 50 rpm. The release data was recorded for up to 24 hours by taking 1 mL of the sample at predefined intervals and restoring the medium with fresh media. Following ultrasound use, the release was also monitored (frequency 2.5 ± 0.1 MHz, insonation time of 1 min). HPLC analysis was performed using the developed method to ascertain the amount of drug present in each sample. Several kinetic models were fit to know the mechanism. The highest correlation coefficient (R^2) was used to determine the most suitable model. The slope and R^2 values were used to calculate the release-exponent value, representing the drug release mechanism.[34]

Ultrasound stability studies

DBF-loaded NBs were exposed to ultrasound at 50 Hz resonance frequency, 30W power, and a standard acoustical pressure gradient of 2.5 ± 0.2 MPa. The ultrasound stimulus frequency was 2.5 ± 0.2 MHz. Ocular microscopy assessed NB structural integrity before and after ultrasound exposure (30 seconds, 1, 2, 3, 4, and 5 min) with a 10-minute rest period at 37 °C.[34] As per the general stability guidelines, DBF nanobubble stability was assessed over one month at various temperatures. Drug amount, encapsulation effectiveness, and mean particle size were measured on the first, tenth, and thirty days.[35]

Determination of haemolytic activity (HA)

The haemolytic potential of drug-loaded NBs was assessed using a 30% v/v human blood cell suspension in pH 7.4 phosphate buffer. Varying v/v ratios of NB preparations (1-10%) were combined with the blood cell suspension. A blank control inducing complete haemolysis was created with excess ammonium chloride. After incubating for two hours at 37 °C, the samples were centrifugated at 3000 rpm for 10 minutes. Subsequently, the supernatant was analysed using a spectrophotometer at a wavelength of 543 nm haemolysis percentage was calculated compared to the 100% haemolysis control.[36] The following formula was used to determine the % haemolysis:

$$\%Hemolysis = \frac{ABS_{Sample} - ABS_0}{ABS_{100} - ABS_0} X\,100$$

Where in ABS_0 and ABS_{100} stands for absorbances of the solution at 0 and 100 % haemolysis, respectively.

Study of cellular uptake

Cells' internalization of a drug and drug-loaded NBs was thoroughly investigated using confocal scanning laser microscopy. HepG2 cells were cultivated for one night in a confocal chamber before being co-cultivated with DBF drug (50 µM dissolved in DMSO), DBF-loaded nanobubbles (50 µM) with no sonication, and DBF-loaded nanobubbles (50 µM) with sonication. With blue-filtered glasses, confocal pictures were taken at various intervals using an excitation wavelength of 405 nm. After mixing the formulations (50 µM) with cell lines, they were cultured continuously for two hours. A luminescent microplate reader was used to measure the fluorescence intensity at emission and excitation wavelengths of 503 nm and 528 nm. Three duplicates of each experiment were carried out.[37]

Cytotoxicity assay for in vitro cells

The HepG2 cells were cultured in DMEM supplemented with 10% FBS at a temperature of 37 °C and 5% CO_2, with a cell density of 5×10^4 cells per well. Different treatments, including blank, DBF solution, and DBF-loaded NBs (50 µM) with and without sonication, were applied in 96-well plates. After 24 and 48 h, MTT (5 mg/mL) was added, and formazan was dissolved in DMSO. The microplate absorbance reader was utilized to determine the absorbance of the samples at a wavelength of 570 nm. Mean ± SD from three or more experiments was statistically analysed with an unpaired Student's t-test ($p<0.05$).[37]

Pharmacokinetic studies

Male Wistar rats (200 ± 20 g, 4-5 weeks) from the Nutrition National Institute (NIN), Telangana, India, were used following the Committee for Control and Supervision of Experiments on Animals (CCSEA) with IAEC approval bearing a protocol number of 1447/PO/Re/S/11/CPCSEA-81/A). Rats acclimated for a week under standard conditions were divided into two groups (n=6). NBs formulation (30 mg/kg BW), vehicle, and DBF (0.25% w/v sodium methylcellulose) were administered orally. Blood samples were collected (250 µL) at regular intervals ranging from 0.25 to 24 hours from the retroorbital plexus, sample consisting of Plasma was obtained, and HPLC was used to analyse the samples.

Data and statistical analysis

The pharmacokinetic parameters were determined using Winnonlin (version 3.1), which involves a non-compartmental method. Mean ± SD stood for the standard deviation of pharmacokinetic variables, and further analysis was performed with GraphPad Prism (GraphPad Software 8.05 Inc., CA).

Results

In this study, Dabrafenib nanobubbles were formed using the solvent evaporation method with an ultrasound. Table 2 defined a clear Quality Target Product Profile (QTPP) for NBs, distinguishing them from conventional products. QbD emphasized a monitoring critical quality attribute (CQAs) to achieve and maintain QTPP. NBs aimed to enhance drug stability, bioavailability, and targeted delivery, addressing solubility and short half-life issues. In this study, PS, PDI, and EE were selected as CQAs. The table succinctly summarized the chosen CQAs and their rationale.

The study involved fifteen runs with three centre points (Table 2). Multiple linear regression analysis (2FI) constructed polynomial models (quadratic, two-factor, and linear). The model selection used R^2, predicted R^2, adjusted R^2, and coefficient of variance (C.V). ANOVA assessed variable impact on responses.

PS

After 15 trials, PS, PDI, and EE ranged from 189.6 to 392.9 nm, 0.301 to 0.693 PDI, and 55.12 to 89.33, respectively, becoming critical for DBF-loaded nanobubbles. The model's F value 1124.15, with a 0.01 percent chance of being noise, confirmed its 'quadratic' nature and significant lack of fit insignificance. ANOVA found variables with p-values below 0.0500 that significantly impacted the response.

The insignificant of the Lack of Fit relative to the pure error was indicated by an F-value of 1.36. It was possible

Table 2. Runs designed for the trails.

Run	Factor 1	Factor 2	Factor 3	Response 1	Response 2	Response 3
	A: Stabilizer concentration	B: Homogenization Speed (HS)	C: Homogenization Duration (HD)	Particle size (PS)	PDI	Entrapment efficiency (EE)
	ratio	rpm	min	nm		%
1	2.5	10000	7.5	214.76	0.345	61.28
2	0.5	10000	7.5	365.2	0.693	78.98
3	0.5	15000	10	392.9	0.688	69.2
4	1.5	15000	7.5	238.3	0.38	67.44
5	0.5	15000	5	230	0.481	66.81
6	1.5	20000	10	250.8	0.343	84.74
7	1.5	15000	7.5	241.7	0.368	68.9
8	2.5	15000	10	198.23	0.312	83.56
9	1.5	15000	7.5	238.2	0.32	68.32
10	2.5	20000	7.5	280.1	0.393	89.33
11	1.5	20000	5	193.2	0.301	61.57
12	0.5	20000	7.5	305.4	0.607	55.12
13	1.5	10000	5	189.6	0.32	76.24
14	2.5	15000	5	244.4	0.361	70.37
15	1.5	10000	10	241.4	0.396	70.74

that a Lack of Fit F-value of this magnitude could arise from noise with a probability of 44.96%. A non-significant lack of fit is good, the model to fit was required. The 3-D surface response (SR) and contour plots (CP) illustrated variable effects on particle size (PS) are depicted in Figure 1.

The R^2 corrected R^2 and anticipated R^2 were 0.9995, 0.9986, and 0.9943, respectively, showed a model precision of 112.395, surpassing the required value of 4. Variables A, B, C, AB, AC, A^2, and C^2 were significant model terms influencing the outcome. They were considered meaningful, and the regression equation was as follows:

PDI

A dimensionless measure of the particle size distribution's broadness is the PDI. Typically, it falls between 0 and 1.[38] Formulations exhibited PDIs from 0.301 to 0.693, with a model F value of 47.54, indicated the significance of the proposed "quadratic" model and an insignificant lack of fit (F-value 0.29).

ANOVA showed significant factors (p-value < 0.0500), leading to the removal of non-significant variables. It was possible that a Lack of Fit F-value of this magnitude could be attributed to noise, with an 83.07% probability. A negligible absence of fit is desirable – the present study aimed for the model to be well-fit. Regression coefficients (R^2, adjusted R^2, and anticipated R^2) were 0.9884, 0.9677, and 0.9254, respectively, showed the model's usefulness with precision exceeding the necessary value (19.943).

Model terms (A, C, AB, AC, A^2, and C^2) had p-values < 0.050, signifying a substantial impact. The resulting regression equation is:

$$\textit{Polydispersity index}\,(PDI) = +0.1560 - 0.1322A - 0.0138B + 0.0345C + 0.0335AB - 0.0640AC - 0.0085BC + 0.1370A^2 + 0.0165B^2 - 0.0325C^2$$

Positive coefficients signify a rise in the associated variable(s), which increases PDI, while negative coefficients indicated a decline, which reduced PDI. All formulations maintained PDI within acceptable bounds, consistently less than 0.4. The graphical image of the 3-D response surface and contour plots illustrated variable effects on the PDI were shown in Figure 2.

Entrapment efficiency (EE)

An impact on EE ranges from 55.12 to 89.33 percent. The model's F value of 143.39, with a 0.01% chance likely due to noise, indicated a significance and negligible fit error for the suggested "quadratic" model. The lack of fit's F-value (2.31) was not statistically significant based on pure error, with a 31.62% probability of being noise. ANOVA identified significant factors (p-value < 0.0500), leading to the removal of non-significant variables.

Response surface and contour plots depicted the impact of variables on EE were shown in Figure 3. Regression coefficients (R^2, adjusted R^2, and anticipated R^2) were 0.9961, 0.9892, and 0.9501, respectively. The predicted R^2 aligned closely with the adequate R^2, differing by 0.2. The model, evidenced by an adequate precision of 43.07, surpassing the necessary value of 4, proved helpful in exploring the design space. Model terms (A, C, AB, AC, BC, B^2, and C^2) had p-values < 0.050, signifying a significant effect. The resulting regression equation is:

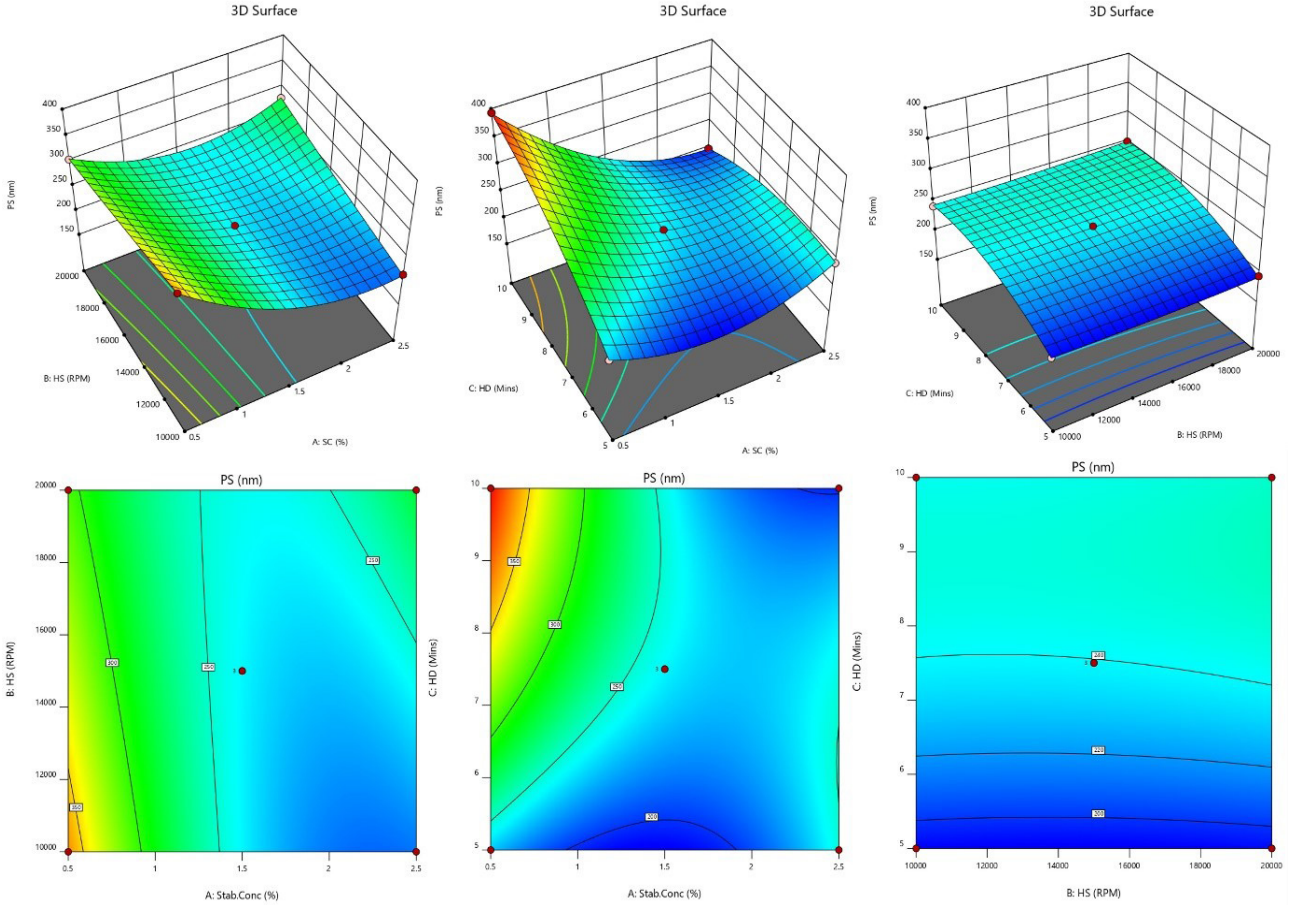

Figure 1. Response surface and contour plots illustrating variable effects on particle size.

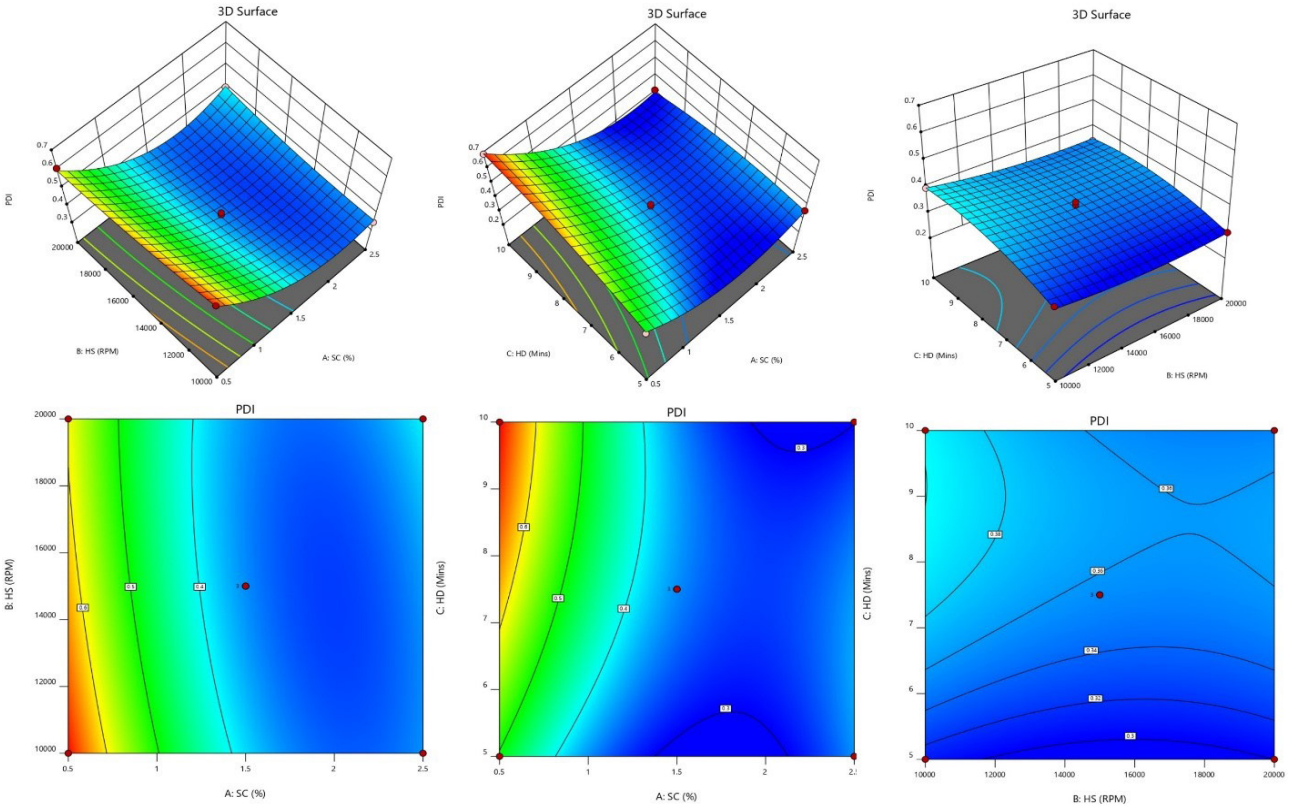

Figure 2. Graphical depiction of response surface and contour plots illustrating variable effects on PDI.

$$\text{Entrapment efficiency}\,(EE) = 68.22 + 34.30A + 0.4400B + 4.16C + 12.98AB + 2.70AC + 7.17BC + 1.06A^2 + 1.90B^2 + 3.20C^2$$

Exploration for optimized formulation

Optimized through the desirability function, the design yielded an optimal formulation (F opt solution) with a maximum attractiveness of 0.969. Optimal parameters included a 2.47% stabilizer ratio, 16430-rpm homogenization speed, and 10 minutes of homogenization duration, aligned with target values for Critical Quality Attributes (CQAs). The designed space was illustrated in Figure 4.

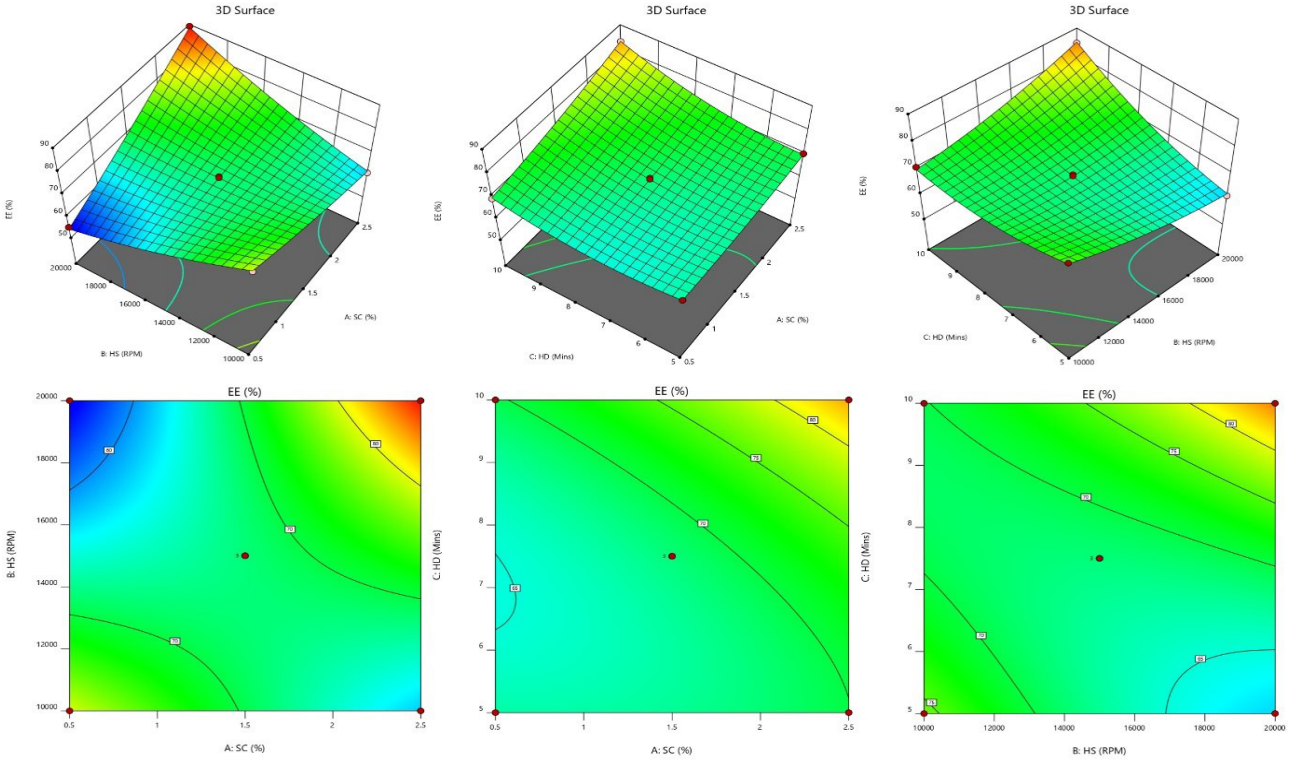

Figure 3. Graphical representation of response surface and contour plots depicted an impact of variables on entrapment efficiency (EE).

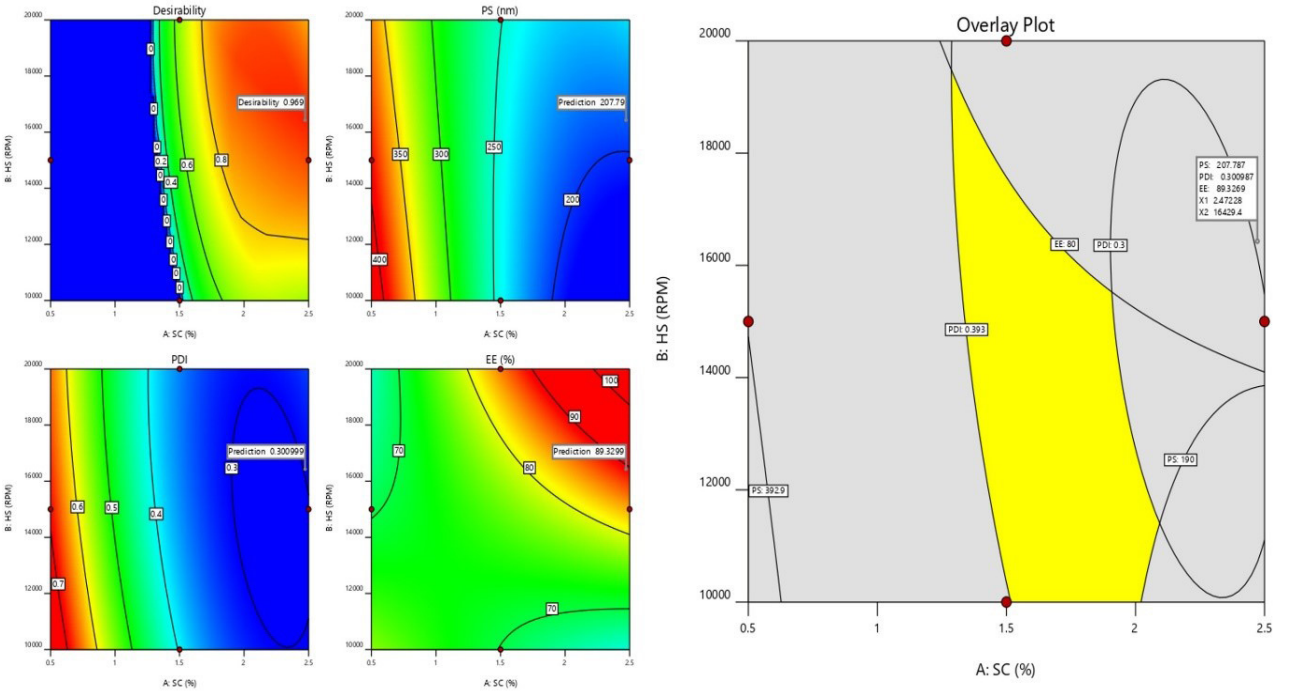

Figure 4. Graphical illustration of desirability and Overlay plot (yellow area denoted feasible region) Design confirmation.

During validation, three checkpoints ensured model robustness and formulation accuracy. Table S1 in Supplementary Data outlined the projected mean standards for size (207.79 nm), PDI (0.301), and EE (89.32) values, which closely matched with observed mean values (190.6 ± 18.4 nm to 0.397 ± 0.096 and 87.21 ± 3.8, respectively). The close alignment between anticipated software values and results from these formulations affirmed the proposed model's validation.

Characterization of nanobubbles (NBs)

Measurements of particle size (PS), polydispersity index (PDI), zeta potential (ZP), and loading capacity (LC)

Particle sizes and uniformity in the formulation remained consistent, with PS and PDI ranging from 190.6 ± 18.4 nm to 0.397 ± 0.096. A polydispersity value below 0.1 to less than 0.4 indicated homogeneity. An optimized formulation's Zeta potential, indicative of colloidal particle surface properties, was -21.4 ± 4.2 mV, with a drug payload of 26.29 ± 4.01. The PS and ZP of the optimized nanobubbles were shown in Figure 5.

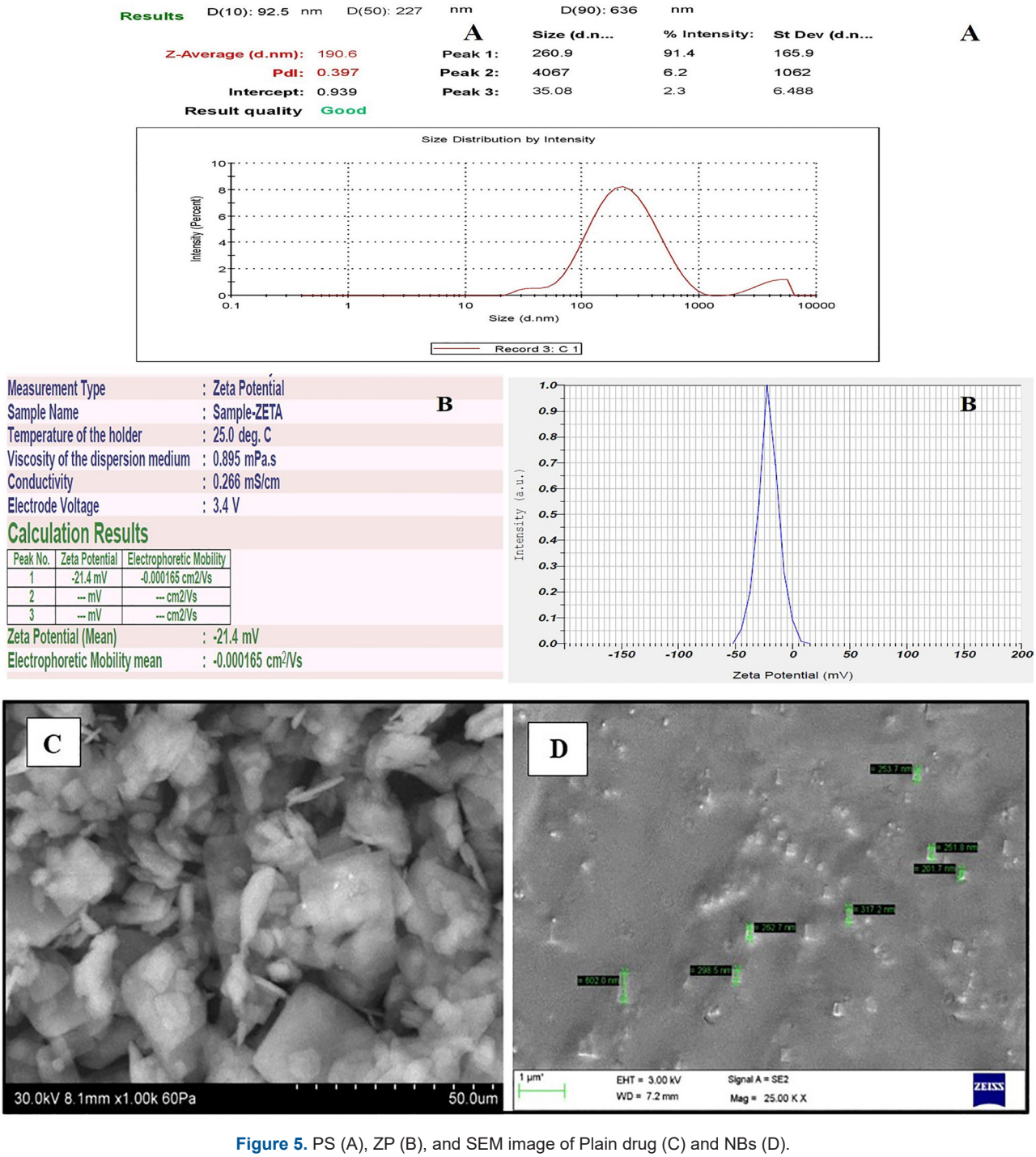

Figure 5. PS (A), ZP (B), and SEM image of Plain drug (C) and NBs (D).

Morphology of NBs

Figure 5 showed the formulation's surface characteristics. In its authentic state, the drug has a broad particle size range with distinct units and an irregular cubic form with micrometre-sized particles. However, after the formation of the NB, the micronized drug particles changed to round nanosized particles with a consistent nano-size range of 207 ± 26 nm.[40]

Fourier transform infrared apectroscopy (FTIR) and differential scanning calorimetry (DSC)

Figure 6 illustrated the component compatibility by recording the nano-formulation, excipients, and plain drug IR spectra. A scanning range of 400 cm^{-1} 1 to 4000 cm^{-1} was used. Characteristic peaks were seen in the plain drug at 2960, 2929, 2791, 2651, 1616,1589,1518, 1458, 1330,1242, 1109, and 1070 cm^{-1}.[39] DSC analysis indicated DBF's melting point with an endothermic peak at 166.88 °C (Figure 6). Endothermic peaks at 57.24 °C and 201.72 °C in the physical mixture correspond to PVA and PLGA melting temperatures. A distinctive endothermic peak at 192.65 °C showed PVA thermal breakdown. Similar melting transitions in drug-loaded and blank nanoparticles suggest unchanged PVA and PLGA during encapsulation,

Drug release

Figure 7 depicted dissolution profiles of plain drug and drug-loaded NBs without and with acoustic aid in pH 7.4 phosphate buffer. After six hours, cumulative drug release (CDR) was 15.51%, 36.88%, and 55.16% for plain drugs, nanobubbles without acoustic, and with acoustic, respectively. By 24 hours, over 95% was released from NBs with acoustic assistance.[33] Regression coefficients for Korsmeyer Peppas (R^2 for formulation without and with acoustic were 0.987 and 0.991), and Higuchi (formulation without and with acoustic were 0.9849 and 0.9614) models suggest strong correlations, while lower coefficients are observed for zero-order (formulation without and with acoustic were 0.8548 and 0.9388) and first-order (formulation without and with acoustic were 0.6052 and 0.6815) models, implying constant rate and exponential decay, respectively.

Ultrasound stability studies

DBF-loaded NBs remained stable at 25 °C and 2.5 MHz ultrasound for five minutes, retained their shape. However, at 37 °C, stability declined, with degradation starting after 3 minutes of sonication and complete depletion by 5 minutes.

Evaluation of the stability of DBF NBs

DBF-loaded nanobubbles (NBs) underwent stability assessments (Table 3). At 4 °C and 25 °C, minimal changes in drug content indicated robustness, with EE showed a slight variation, suggesting protection against degradation. However, a notable reduction in entrapment occurred at elevated temperatures, indicating structural disruption. Throughout the experiment, PDI values remained below 0.3, highlighting the stability and uniformity of DBF nanobubbles.

Determination of haemolytic activity

Haemolytic activity (HA) evaluation at 10 mg/mL

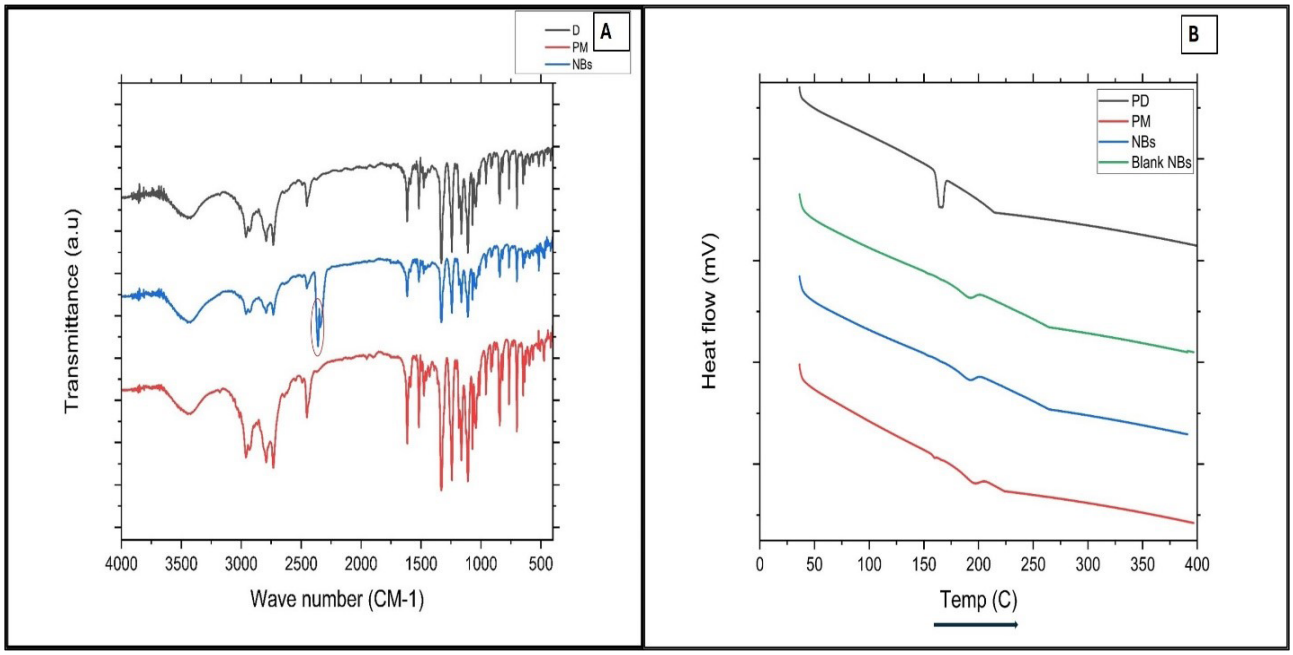

Figure 6. A) FTIR overlay of a) D (black line- Drug), b) NBs (Blue line-Nanobubbles) and c) PM (Red line- physical mixture. B) Overlay of DSC thermograms of a) Drug (Black line- drug or PD (plain drug), b) PM (Red line- physical mixture), c) NBs (Blue line- Nanobubbles) and d) Blank NBs (Green line- blank nanobubbles).

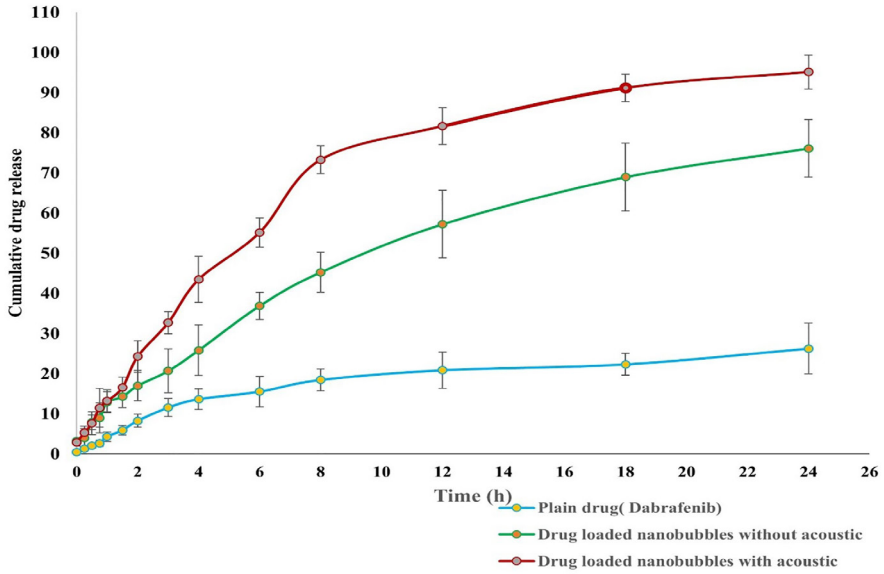

Figure 7. In-vitro drug release displayed in the presence and absence of ultrasound aid.

concentration confirmed the safety of both blank NBs and DBF-loaded NBs. PLGA NBs aqueous solutions showed no haemolytic activity, and drug-loaded NBs demonstrated excellent safety with erythrocytes.

Study of cellular uptake

Fluorescence intensity analysis was employed to assess the internalization of dabrafenib from nanobubbles in HepG2 cells. The findings on fluorescence intensity obtained during a 2-hour incubation were shown in Figure 8A and the images of the same was shown in Figure S1 (Supplementary Data). HepG2 cells that received DBF-loaded NBs in addition to ultrasound showed a mean fluorescence intensity of 6.97, 1.5 times higher than cells treated with DBF-loaded NBs alone.

Cytotoxicity assay for in vitro cells

Figure 8B illustrated that the MTT assay was used to evaluate the in vitro cytotoxicity of nanobubbles (NBs) loaded with dabrafenib on HepG2 cells. Both plain drug and formulations at lower concentrations resulted in over 98% cell vitality. Nevertheless, when administered at a concentration of 20 µM, cell viability decreased to less than 85%, potentially falling below the minimum effective concentration. Of the three formulations, nanobubbles combined with ultrasound proved the lowest cell viability with increasing concentration. Individual IC50 values were 90.81 µM, 76.24 µM, and 68.54 µM for free drug, NBs without ultrasound, and NBs with ultrasound, respectively.

Pharmacokinetic studies

Figure 9 illustrated the plasma concentration-time curve for plain drug (PD) suspension (0.25% w/v sodium methylcellulose) and the optimized NBs. Table 4 provided pharmacokinetic information, and the DBF plasma nanobubbles formulation displayed a significantly higher area under the curve levels than the pure drug treatment. The retention time for the drug and internal standard

Table 3. PS, PDI, and EE Drug loaded NBs stored at different temperatures.

	F_{opt}	Initial	On 15th day	On 30th day
4ºC	PS (nm)	190.6 (±18.4)	192.71 (±10.45)	194.86 (±14.01)
	PDI	0.397 (±0.096)	0.364 (±0.098)	0.389 (±0.052)
	EE (%)	87.21 (±3.8)	87.56 (±4.15)	85.86 (±6.34)
25ºC	PS (nm)	190.6 (±18.4)	194.66 (±13.48)	199.4 (±6.38)
	PDI	0.397 (±0.096)	0.304 (±0.048)	0.363 (±0.067)
	EE (%)	87.21 (±3.8)	86.33 (±5.06)	85.58 (± 4.25)
40ºC	PS (nm)	190.6 (±18.4)	194.26 (±14.36)	200.86 (±10.10)
	PDI	0.397 (±0.096)	0.378 (±0.029)	0.384 (±0.044)
	EE (%)	87.21 (±3.8)	85.28 (±4.46)	83.8 (±6.12)

Note: F_{opt} formulation, n=3 (*p<0.05%).

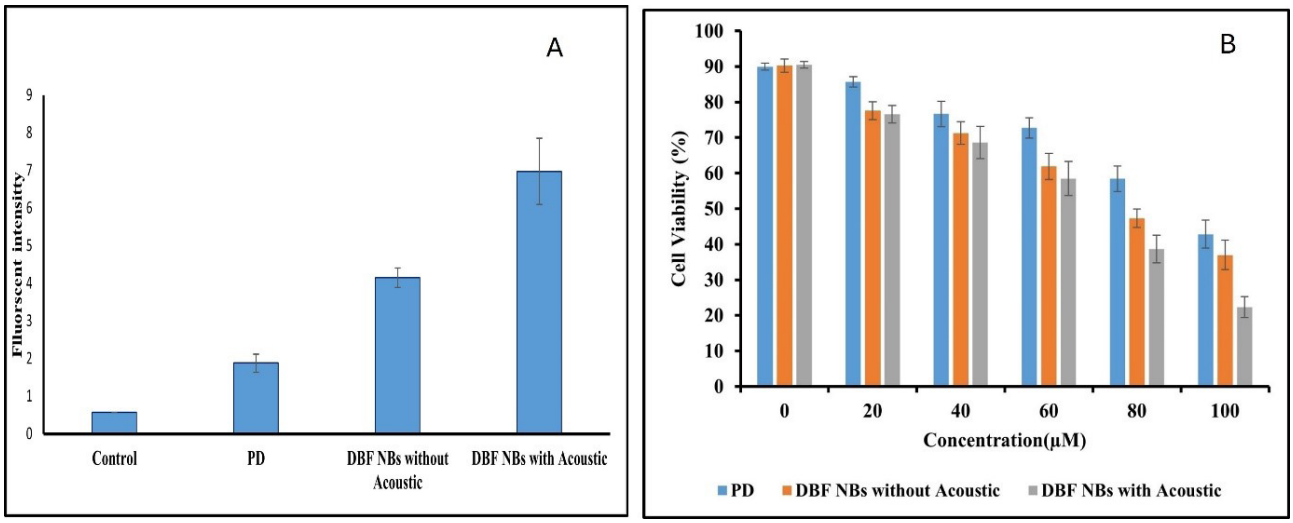

Figure 8. A) Graphical representation of cellular uptake. (n=3). B) In vitro cytotoxicity of control (cells that have not been exposed to any treatment or test substances), plain drug, drug loaded NBs without ultrasound, and with ultrasound.

(Sorafenib) was 9.22 min and 11.41 min, respectively. The maximum concentration (C_{max}) (4.74-fold) and the Area under the curve (AUC_{0-t}) (6.82-fold) of NBs were substantially higher than the plain drug.

Discussion

In this study, DBF-loaded PLGA NBs were formulated using the solvent evaporation method, with optimization conducted through the BBD. The term "nanobubbles" simplified the more exact "nanodroplets" due to octa fluoro-propane fluidity at room temperature. The liquid-to-vapor phase transition induced by ultrasound, called acoustic droplet vaporization, transforms nanodroplets into nanobubbles, emphasized their echogenic qualities

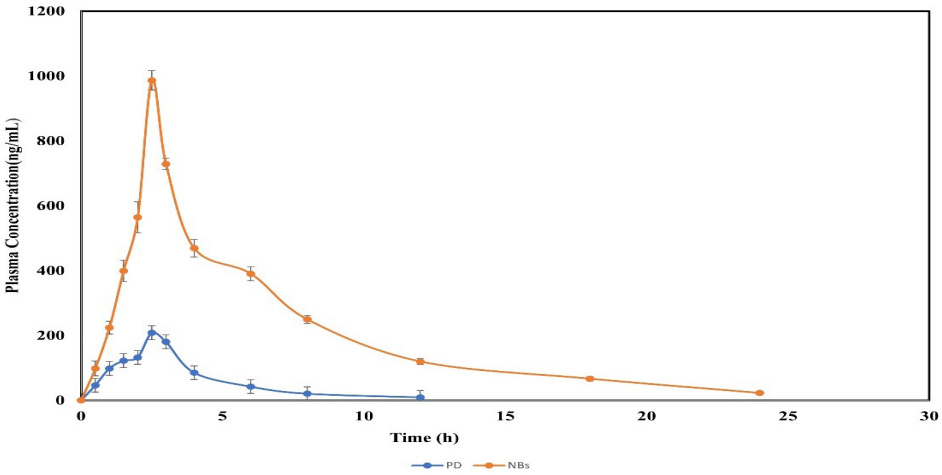

Figure 9. Mean plasma concentration-time curves of Dabrafenib in Male Wistar rats (n = 6, ± SD) after oral administration of 30 mg/kg BW of DBF -suspension and DBF-loaded NBs.

Table 4. Pharmacokinetic parameters.

Pharmacokinetic parameters	Dabrafenib Pure drug	Dabrafenib loaded NBs
C_{max} (ng/mL)	208.15 ± 34.04	987.06 ± 81.21
T_{max} (h)	2.5	2.5
Half-life (h)	2.506 ± 0.54	4.622 ± 0.68
AUC_{0-t} (ng. h/mL)	730.4451 ± 84.98	4982.857 ± 228.43
AUC_{0-inf} (ng. h/mL)	763.636 ±105.12	5134.57 ± 378.45
Ke (h^{-1})	0.2765	0.1499

in ultrasonography images.[41,42] "Ultrasound" denotes pressure waves with compressional and rarefactional fluctuations at frequencies ≥20 kHz. Its effects include cavitation for bubble size reduction and sonoporation, facilitating the uptake of the diminished bubble.[43] NBs are emerging as a formulation strategy because of their targeting ability. The formulated PLGA NBs of dabrafenib can utilize natural physiological processes, such as the enhanced permeability and retention effect, to accumulate passively within diseased tissues. This, in turn, improved the efficiency of targeting.[44] A combination of ultrasound and NBs helped in drug localization while overcoming the off-target adverse effects.[45]

The quadratic model suggested by design was applied to PS, PDI, and EE. Positive coefficients in the model indicated a positive connection, signifying that increased associated variables led to higher entrapment efficiency. Contour and 3D plots showed that higher and lower stabilizer concentrations influenced particle size due to uncontrolled nuclei diffusion at lower concentrations. All formulations maintained PDI within acceptable limits (less than 0.4).[46] Stirring rates affected PDI, with higher rates initially resulting in more mono dispersity, but further stirring caused agglomeration due to reduced repulsive forces.

The FTIR peaks for the drug were observed at 2960 and 2929 cm^{-1} are indicative of C-H stretching vibrations associated with methyl and methylene groups, while the peak at 2791 cm^{-1} was attributed to C-H stretching of methyl groups specifically. A peak at 2651 cm^{-1} points to weakly interacting C-H groups. The presence of aromatic characteristics is confirmed by peaks at 1616 and 1589 cm^{-1}, which corresponded to C=C stretching within aromatic rings. Furthermore, the peak at 1518 cm^{-1} reinforced the existence of aromatic C-H bending. Peaks at 1458 and 1330 cm^{-1} are associated with C-H bending vibrations found in both aliphatic and aromatic structures. Additionally, the peaks at 1242, 1109, and 1070 cm^{-1} indicated C-O stretching vibrations, suggested the presence of ester, ether, or alcohol functional groups. In case of NBs an additional peak at 2400-2450 cm^{-1} associated with the C=O stretching vibration of the carboxyl group (–COOH) or the carbonyl group (–C=O) of the polymer structure is observed. This indicated potential physical interactions or bonding between dabrafenib and PLGA nanobubbles, as these groups could facilitate binding through non-covalent interactions. The presence of this peak suggested that the carbonyl functionality in PLGA may play a role in the physical association with the drug.[39] DSC revealed no distinct drug peak in the formulation, indicated the absence of crystalline drug material.[30] SEM analysis displayed a homogeneous, smooth, spherical-shaped nanobubbles.[40]

Drug release occurred due to collapse cavitation induced by acoustic waves, disrupting nanobubble structures and enabling rapid medication release. Acoustic waves, regulated and non-invasive, offered precise medicine administration and targeting. Ultrasound stability studies indicated the transformation of the gas core from nanodroplets to bubbles, known as acoustic droplet generation.[47,48] Release from nanobubbles was significantly higher than a simple drug suspension. Notably, ultrasound assistance increased the drug release. The drug release mechanism from the NBs followed Korsmeyer–Peppas model and Higuchi model, uncovering an atypical release pattern mainly controlled by diffusion of drug from the NBs. Studies suggested that regulated and non-invasive acoustic waves are ideal for precise drug administration and targeting as seen from the *in vitro* drug release studies.[49] A haemolytic analysis is imperative, even with the oral delivery of nanobubbles. It guarantees the safety and compatibility of the product by examining any possible negative impacts on blood cells, even though the nanobubbles enter the bloodstream following absorption in the gastrointestinal tract. This assessment is vital in averting issues like anaemia or blood clotting, affirming the appropriateness of using nanobubbles orally in medical practice.

The lack of haemolytic properties has proven biocompatibility. Cellular uptake studies highlighted improved absorption of dabrafenib from the nanobubble formulation facilitated by ultrasound.[50]

Enhanced cytotoxicity was attributed to nanobubble size, enabling better drug penetration into cells.[51] During the stability studies it can be ascertained that the small diameters of NBs may contribute to transitions at higher temperature values.[52,53] *In vivo* studies in Wistar rats revealed gradual drug release from the formulation, leading to an increased time to reach maximum concentration (t max) sustained the release of drug for a longer time with prolonged circulation and they help in the disruption of cell membrane. A combination of ultrasound with NBs has helped in destroying tumour cell noninvasively.[54] Our findings proved a significant improvement in the oral bioavailability of the chosen medicine using nanobubbles as compared to plain drug, attributed to increased drug circulation at the nanoscale and enhanced penetration by the polymeric carrier system.

Conclusion

This study emphasized an efficient utilization of nanobubbles for the targeted delivery of the anticancer drug dabrafenib. This optimization resulted in improved solubility and dissolution profiles. The nanobubbles achieved a uniform size distribution using response surface methodology, ensuring their effectiveness. In comparison to regular drug suspensions, DBF NBs demonstrated superior stability and dissolution in the gastrointestinal tract, suggested a potential increase in the drug's half-life. These findings highlighted the potential of PLGA nanobubbles as a valuable tool in ultrasound-responsive formulations for cancer therapy. They offered advantages such as increased solubility and enhanced dissolution, improving oral bioavailability. Additionally, the ability of nanodroplets to transform into nanobubbles through

acoustic droplet vaporization displays their echogenic properties in ultrasonography, further emphasizing their potential in targeted medicine delivery. This study sets the foundation for utilizing nanobubbles to develop ultrasonic-responsive combinations for targeted drug delivery in diseases like chronic myeloid leukaemia.

Ethical Issues

Animal study followed the "Guidelines for Care and Use of Laboratory Animals," and the Institutional Animal Ethics Committee (IAEC) approved the protocols bearing a number 1447/PO/Re/S/11/CCSEA-81/A.

Author Contributions

Bijili Vijaya Laxmi: Conceptualization, Methodology, Validation, Data Curation, Writing - Original Draft. Darna Bhikshapathi: Visualization, Supervision, Writing - Review & Editing. Penakalapati Sailaja Rao: Writing - Review & Editing.

Conflict of Interest

The authors declare no competing interests and also confirm that this research received no external funding.

Supplementary Data

Supplementary data are available at https://doi.org/10.34172/PS.024.40626.

References

1. Kelly CM, Power DG, Lichtman SM. Targeted therapy in older patients with solid tumors. J Clin Oncol. 2014; 32:2635-46. doi:10.1200/JCO.2014.55.4246
2. Kanamala M, Wilson WR, Yang M, Palmer BD, Wu Z. Mechanisms and biomaterials in pH-responsive tumour targeted drug delivery: A review. Biomaterials. 2016;85:152-67. doi:10.1016/j.biomaterials.2016.01.061
3. Chen EM, Quijano AR, Seo YE, Jackson C, Josowitz AD, Noorbakhsh S. Biodegradable PEG-poly(ω-pentadecalactone-co-p-dioxanone) nanoparticles for enhanced and sustained drug delivery to treat brain tumors. Biomaterials. 2018;178:193-203. doi:10.1016/J.BIOMATERIALS.2018.06.024
4. Markman JL, Rekechenetskiy A, Holler E, Ljubimova JY. Nanomedicine therapeutic approaches to overcome cancer drug resistance. Adv Drug Deliv Rev. 2013;65:1866-79. doi:10.1016/j.addr.2013.09.019
5. Kim YS, Kim BG, Rhim H, Bae DS, Lee JW, Kim TJ, et al. Uterine fibroids: Semiquantitative perfusion MR imaging parameters associated with the intraprocedural and immediate postprocedural treatment efficiencies of MR imaging-guided high-intensity focused ultrasound ablation. Radiology. 2014;273:462-471.doi:10.1148/radiol.14132719
6. Liu J, Han J, Kang Z, Golamaully R, Xu N, Li H, et al. In vivo near-infrared photothermal therapy and computed tomography imaging of cancer cells using novel tungsten-based theranostic probe. Nanoscale. 2014;6:5770-6. doi:10.1039/c3nr06292a
7. Borregaard R, Lukac P, Gerdes C, MØller D, Mortensen PT, Pedersen L. Radiofrequency ablation of accessory pathways in patients with the Wolff-Parkinson-White syndrome: The long-term mortality and risk of atrial fibrillation. Europace. 2016;17:117-122. doi:10.1093/europace/euu176
8. Zhang P, Hu C, Ran W, Meng J, Yin Q, Li Y. Recent progress in light-triggered nanotheranostics for cancer treatment. Theranostics. 2016;6:948-968. doi:10.7150/thno.15217
9. Lukianova-Hleb E, Hu Y, Latterini L, Tarpani L, Lee S, Drezek RA. Plasmonic nanobubbles as transient vapor nanobubbles generated around plasmonic nanoparticles. ACS Nano. 2010;4:2109-23. doi:10.1021/nn1000222
10. Kinfe T, Stadlbauer A, Winder K, Hurlemann R, Buchfelder M. Incisionless MR-guided focused ultrasound: technical considerations and current therapeutic approaches in psychiatric disorders. Expert Rev Neurother. 2020;20:687-96. doi:10.1080/14737175.2020.1779590
11. Lee J, Min HS, You DG, Kim K, Kwon LC, Rhim T, et al. Theranostic gas-generating nanoparticles for targeted ultrasound imaging and treatment of neuroblastoma. J Control Release. 2016;223:197-206. doi:10.1016/j.jconrel.2015.12.051
12. McDannold N, Zhang Y, Supko GJ, Power C, Sun T, Peng C, et al. Acoustic feedback enables safe and reliable carboplatin delivery across the blood-brain barrier with a clinical focused ultrasound system and improves survival in a rat glioma model. Theranostics. 2019; 9:6284–6299. Doi:10.7150/thno.35892
13. Sirsi SR, Borden MA. Microbubble compositions, properties and biomedical applications. Bubble Sci Eng Technol. 2009;1:3-17. Doi:10.1179/175889709X446507.
14. Lu Y, Wang J, Huang R, Chen G, Zhong L, Shen S. Microbubble-mediated sonothrombolysis improves outcome after thrombotic microembolism-induced acute ischemic stroke. Stroke. 2016;47:1344-53. doi:10.1161/STROKEAHA.115.012056
15. Hong D, Yang J, Guo J, Zhang Y, Chen Z. Ultrasound-targeted microbubble destruction enhances inhibitory effect of apatinib on angiogenesis in triple negative breast carcinoma xenografts. Anal Cell Pathol. 2021;2021:8837950. doi:10.1155/2021/8837950
16. Wang J, Zhao Z, Shen S, Zhang C, Guo S, Lu Y, et al. Selective depletion of tumor neovasculature by microbubble destruction with appropriate ultrasound pressure. Int J Cancer. 2015;137:2478-91. doi:10.1002/ijc.29597
17. Ehlerding EB, Grodzinski P, Cai W, Liu CH. Big potential from small agents: nanoparticles for imaging-based companion diagnostics. ACS Nano. 2018; 12 :2106-21. doi:10.1021/acsnano.7b07252

18. Yang H, Deng L, Li T, et al. Multifunctional PLGA nanobubbles as theranostic agents: Combining doxorubicin and P-gp siRNA co-delivery into human breast cancer cells and ultrasound cellular imaging. J Biomed Nanotechnol. 2015;11:2124-36. doi: 10.1166/jbn.2015.2168
19. Acharya S, Sahoo S. PLGA nanoparticles containing various anticancer agents and tumour delivery by EPR effect. Adv Drug Deliv Rev. 2011;63:170-183. doi:10.1016/j.addr.2010.10.008.
20. Sun Y, Zheng Y, Ran H, Zhou Y, Shen H, Chen Y. Superparamagnetic PLGA-iron oxide microcapsules for dual-modality US/MR imaging and high intensity focused US breast cancer ablation. Biomaterials. 2012;33:5854-64. doi:10.1016/j.biomaterials.2012.04.062
21. Zhou Y, Wang Z, Chen Y, ShenH, Luo Z, Li A, et al. Microbubbles from gas-generating perfluorohexane nanoemulsions for targeted temperature-sensitive ultrasonography and synergistic HIFU ablation of tumors. Adv Mater. 2013;25:4123-30. doi:10.1002/adma.201301655
22. Falchook GS, Long GV, Kurzrock R, Kim KB, Arkenau TH, Brown MP, et al. Dabrafenib in patients with melanoma, untreated brain metastases, and other solid tumours: a phase 1 dose-escalation trial. Lancet. 2012;379:1893-1901. doi:10.1016/S0140-6736(12)60398-5
23. Dahan A, Miller JM, Amidon GL. Prediction of solubility and permeability class membership: Provisional BCS classification of the world's top oral drugs. AAPS J. 2009;11:740-46. doi:10.1208/s12248-009-9144-x
24. Kasim NA, Whitehouse M, Ramachandran C, Bermejo M, Lennernäs H, Hussain AS, Molecular properties of WHO essential drugs and provisional biopharmaceutical classification. Mol Pharm. 2014;1:85-96. doi:10.1021/mp034006h
25. Kumari P, Ghosh B, Biswas S. Nanocarriers for cancer-targeted drug delivery. J Drug Target. 2016;24:179-91. doi:10.3109/1061186X.2015.1051049
26. Gao J, Liu J, Meng Z, Li Y, Hong Y, Wang L, et al. Ultrasound-assisted C3F8-filled PLGA nanobubbles for enhanced FGF21 delivery and improved prophylactic treatment of diabetic cardiomyopathy. Acta Biomater. 2021;130:395-408. doi:10.1016/j.actbio.2021.06.015
27. Cui W, Bei J, Wang S, Zhi G, Zhao Y, Zhou X. Preparation and evaluation of poly(L-lactide-co-glycolide) (PLGA) microbubbles as a contrast agent for myocardial contrast echocardiography. J Biomed Mater Res Part B Appl Biomater. 2020;73:171-8. doi:10.1002/jbm.b.30189
28. Rangara N, Pailla SR, Chowta P, Sampathi S. Fabrication of Ibrutinib Nanosuspension by Quality by Design Approach: Intended for Enhanced Oral Bioavailability and Diminished Fast Fed Variability, AAPS PharmSciTech. 2019;20(8):326. doi:10.1208/s12249-019-1524-7
29. Wang B, Lu X, Tao S, Ren Y, Gao W, Liu X, Yang B. Preparation and properties of CO_2 micro-nanobubble water based on response surface methodology, Appl Sci. 2021;11(24):11638. doi:10.3390/app112411638
30. Rai SK, Gunnam A, Mannava MKC, Nangia AK. Improving the dissolution rate of the anticancer drug dabrafenib. Cryst. Growth Des. 2020;20:1035-46. doi:10.1021/acs.cgd.9b01365
31. Ponnaganti M, Kishore Babu A. Preparation, characterization and evaluation of chitosan nanobubbles for targeted delivery of ibrutinib. nat volatiles essent oils. Nat Volatiles Essent Oils. 2021;8(6):5017-37.
32. Başpınar Y, Erel-Akbaba G, Kotmakçı M, Akbaba H. Development and characterization of nanobubbles containing paclitaxel and survivin inhibitor YM155 against lung cancer. Int J Pharm. 2019;566:149-56. doi:10.1016/j.ijpharm.2019.05.039.
33. Pailla SR, Talluri S, Rangaraj N, Ramavath R, ChallaV S, Doijad N, et al. Intranasal Zotepine Nanosuspension: intended for improved brain distribution in rats. Daru. 2019;27(2):541-56. doi:10.1007/s40199-019-00281-4
34. Yang H, Shen X, Yan J, Xie X, Chen Z, Li T, et al. Charge-reversal-functionalized PLGA nanobubbles as theranostic agents for ultrasonic-imaging-guided combination therapy. Biomater Sci. 2018;6:2426-39. doi:10.1039/c8bm00419f
35. Hernandez C, Abenojar EC, Hadley J, De Leon AC, Coyne R, Perera R. Sink or float? Characterization of shell-stabilized bulk nanobubbles using a resonant mass measurement technique. Nanoscale. 2019;11:851-5. doi:10.1039/c8nr08763f
36. Wang L, Zhang J, Hu. Generation and stability of bulk nanobubbles: A review and perspective, Curr Opin Colloid Interface Sci. 2021;53(1):101439. doi:10.1016/j.cocis.2021.101439.
37. Takano S, Kondo H. Quantitative Method for Determination of Hemolytic Activity of Clostridium Septicum Toxin. Japanese J Med Sci Biol. 1987;40:47-59. doi:10.7883/yoken1952.40.47
38. Zhang Y, Liu AT, Cornejo YR, van Haute D, Berlin JM. A Systematic comparison of in vitro cell uptake and in vivo biodistribution for three classes of gold nanoparticles with saturated PEG coatings. PLoS One. 2020;15(7):e0234916. doi:10.1371/journal.pone.0234916
39. Cho MH, Niles A, Huang R, Inglese J, Austin CP, Riss T, et al. A bioluminescent cytotoxicity assay for assessment of membrane integrity using a proteolytic biomarker. Toxicol Vitr. 2008;22(4):1099-106. doi:10.1016/j.tiv.2008.02.013
40. Burgess MT, Porter TM. Control of acoustic cavitation for efficient sonoporation with phase-shift nanoemulsions. Ultrasound Med Biol. 2019;45:846-58. doi:10.1016/j.ultrasmedbio.2018.12.001
41. Kripfgans OD, Fabiilli ML, Carson PL, Fowlkes

JB. On the acoustic vaporization of micrometer-sized droplets. J Acoust Soc Am. 2004;116:272-81. doi:10.1121/1.1755236
42. Ayodele AT, Valizadeh A, Adabi M, Esnaashari SS, Madani F, Khosravani M, et al. Ultrasound nanobubbles and their applications as theranostic agents in cancer therapy: A review. Biointerface Res Appl Chem. 2017;7:2253-62
43. Danaei M, Dehghankhold M, Ataei S, Hasanzadeh Davarani F, Javanmard R, Dokhani A, et al. Impact of particle size and polydispersity index on the clinical applications of lipidic nanocarrier systems. Pharmaceutics. 2018;10(2):57. doi:10.3390/pharmaceutics10020057
44. Kishore Kumar M, Jaya Prakash D, Basava Rao VV. Chitosan nanobubbles development and evaluation for the delivery of sunitinib-an anticancer agent. Int J Appl Pharm. 2022;14:58-67. doi:10.22159/IJAP.2022V14I6.45821
45. Running L, Espinal R, Hepel M. Controlled release of targeted chemotherapeutic drug dabrafenib for melanoma cancers monitored using surface-enhanced Raman scattering (SERS) spectroscopy. Mediterr J Chem. 2018;7:18-27. doi:10.13171/mjc71/01803171500-hepel
46. Yang H, Deng L, Li T, Shen X, Yan J, Zuo L, et al. Multifunctional PLGA nanobubbles as theranostic agents: Combining doxorubicin and P-gp siRNA co-delivery into human breast cancer cells and ultrasound cellular imaging. J Biomed Nanotechnol. 2021;11:2124-36. doi:10.1166/jbn.2015.2168
47. Nirmalkar N, Pacek AW, Barigou M. On the existence and stability of bulk nanobubbles. Langmuir. 2018;34(37):10964-73. doi:10.1021/acs.langmuir.8b01163
48. Li M, Ma X, Eisener J, Pfeiffer P, Ohl CD, Sun C. How bulk nanobubbles are stable over a wide range of temperatures. J Colloid Interface Sci. 2021;596:184-198. doi:10.1016/j.jcis.2021.03.064
49. Hirsch V, Kinnear C, Moniatte M, Rothen-Rutishauser B, Clift MJ, Fink A. Surface charge of polymer coated SPIONs influences the serum protein adsorption, colloidal stability and subsequent cell interaction in vitro. Nanoscale. 2013;5(9):3723-32. doi:10.1039/c2nr33134a.
50. Alheshibri M, Al Baroot A, Shui L, Zhang M. Nanobubbles and nanoparticles. Curr Opin Colloid Interface Sci. 2021;55:101470. doi:10.1016/j.cocis.2021.101470
51. Kanematsu W, Tuziuti T, Yasui K. The influence of storage conditions and container materials on the long term stability of bulk nanobubbles — Consideration from a perspective of interactions between bubbles and surroundings. Chem Eng Sci. 2020;219:115594. doi:10.1016/j.ces.2020.115594
52. Capolla S, Argenziano M, Bozzer S, Agaro TD, Bittolo T, De Leo L, et al. Targeted chitosan nanobubbles as a strategy to down-regulate microRNA-17 into B-cell lymphoma models. Front Immunol. 2013;14:1200310. doi:10.3389/fimmu.2023.1200310
53. Sandhya P, Poornima P, Bhikshapathi DVRN. Self nanoemulsifying drug delivery system of sorafenib tosylate: development and in vivo studies. Pharm Nanotechnol. 2020;8(6):471-84. doi:10.2174/2211738508666201016151406
54. Cai X, Jiang Y, Lin M, Zhang J, Guo H, Yang F, et al. Ultrasound-responsive materials for drug/gene delivery. Front Pharmacol. 2020;10:1650. doi:10.3389/fphar.2019.01650